

gave signals that were within 15% of the prediction made using the axial behavior of Fig. 3(a) and a R_d/r law for the current density. The rather poor divergence angles obtained in this experiment are probably due to the coarse plasma surface on the anode. With the geometry in question, it would be expected that the radial divergence would be greater than the axial divergence.

The major result of these initial investigations is that intense ion beams can be controlled geometrically and that propagation in a high vacuum, field free region to a first-order focus is governed by single particle trajectories with no evidence of space charge effects. Although the focused current density was not as high as we had hoped, the problems involved appear amenable to solution. We plan to optimize the system with the following modifications:

(a) Plasma sources localized over the slots will be used to maximize the total system efficiency to keep the diode voltage up while extracting a large number of protons into the propagation volume. (b) The capacitive division of the plasma anode in azimuth will be considerably increased, reducing the radial divergence angle. (c) Experiments will be performed using a weak negative bias magnetic field inside the propagation volume. If the total flux inside the anode is zero, all protons, independent of the diode voltage, will arrive at the axis in the absence of radial divergence. In this case, neutralizing electrons will be supplied axially along field lines,

as in previous work.^{1,11}

This work was supported by Sandia Laboratories and the Office of Naval Research.

¹S. Humphries, R. N. Sudan, and L. Wiley, *J. Appl. Phys.* **47**, 2382 (1976).

²P. Dreike, C. Eichenberger, S. Humphries, and R. N. Sudan, *J. Appl. Phys.* **47**, 85 (1976).

³F. Winterberg, *Plasma Phys.* **17**, 69 (1975).

⁴M. J. Clauser, *Phys. Rev. Lett.* **35**, 848 (1975).

⁵A. W. Maschke, *Bull. Am. Phys. Soc.* **21**, 1060 (1976).

⁶H. I. Milde and N. W. Harris, in *Proceedings of the Thirteenth Symposium on Electron, Ion and Photon Beam Technology*, edited by R. F. W. Pease and J. G. Skinner (American Institute of Physics, New York, 1975), p. 1188.

⁷In order to make a large-area plasma by surface electrical breakdown, a sheet of hydrocarbon insulator backed by a metal anode is divided by an array of metal pins inserted into the insulator and flush with its outer surface. Electrical breakdown is initiated on application of the pulsed diode voltage at the pins by fringing fields, and the surface surrounding each pin is capacitively coupled to the cathode.

⁸For a discussion of the theory of these probes at high ion-current density, see C. Eichenberger, S. Humphries, J. Maenchen, and R. N. Sudan, to be published.

⁹R. N. Sudan and R. V. Lovelace, *Phys. Rev. Lett.* **31**, 1174 (1973).

¹⁰K. D. Bergeron, *Appl. Phys. Lett.* **28**, 306 (1976).

¹¹S. Humphries, C. Eichenberger, and R. N. Sudan, to be published.

Experimental Observation of Explosive Instability Due to a Helical Electron Beam^(a)

R. Sugaya, M. Sugawa, and H. Nomoto

Department of Physics, Faculty of Science, Ehime University, Matsuyama, Japan

(Received 9 February 1977)

We have performed experiments on explosive instability of space-charge waves of the helical electron beam due to nonlinear wave-particle interaction. The fast and slow beam modes interact nonlinearly with the helical electron beam and grow simultaneously.

Explosive instability is one of the most interesting phenomena in nonlinear plasma theory,^{1,2} but experimental results supporting such theory have been lacking.³ Further, an experimental study on explosive instability due to nonlinear wave-particle interaction (nonlinear Landau damping) has yet to be reported, although the experimental investigations of the nonlinear Landau damping of nonexplosive type have been given by many authors.⁴⁻⁶ In this Letter, we report the experimen-

tal observation of the explosive instability due to the nonlinear Landau damping.

For an electron beam-plasma system in a magnetic field, the resonant condition for nonlinear wave-particle interaction of two waves with the electron beam is given by^{4,6}

$$\omega_1 - \omega_2 - (k_{\parallel 1} - k_{\parallel 2})v_b = m\omega_c, \quad (1)$$

where v_b is the velocity of the beam, ω_c the electron cyclotron frequency, m an integer, and the

other notations are standard. When the electron beam is not helical, this nonlinear Landau damping is nonexplosive type, as we reported earlier.⁶ However, it has been predicted theoretically that when the beam is helical, the first wave (ω_1) is a positive-energy one, and the second wave (ω_2) is a negative-energy one ($\omega_1 > \omega_2$; $m > 0$), the nonlinear Landau damping is possibly an explosive type.² In our experiments, we observed that the fast and slow space-charge waves of the helical electron beam (fast and slow beam modes) which correspond to the positive- and negative-energy ones, respectively, are amplified simultaneously by the nonlinear interaction with the beam.

Based on the general kinetic equations derived by Porkolab and Chang,² we obtained the following kinetic equations for the explosive instability of the fast and slow beam modes:

$$\frac{\partial |E_{\omega_1}|^2}{\partial t} = -2\gamma_1 |E_{\omega_1}|^2 + \alpha_1 |E_{\omega_1}|^2 |E_{\omega_2}|^2, \quad (2)$$

$$\frac{\partial |E_{\omega_2}|^2}{\partial t} = -2\gamma_2 |E_{\omega_2}|^2 + \alpha_2 |E_{\omega_1}|^2 |E_{\omega_2}|^2, \quad (3)$$

with nonlinear wave-particle coupling coefficients given as follows:

$$\alpha_1 \left| \frac{\partial \epsilon}{\partial \omega_2} \right| = \alpha_2 \left| \frac{\partial \epsilon}{\partial \omega_1} \right| = \frac{2(\omega_b/\omega_c)^4 k_{\perp 1}^4 k_{\perp 2}^2}{9\pi^{1/2} k_1^2 k_2^2 m_e n_b |k_{\parallel}| v_{tb} \omega_c}, \quad (4)$$

where it is assumed that $k_{\perp} v_{0\perp}/\omega_c \ll 1$, and the dispersion relation of two waves is given by⁷

$$\omega - k_{\parallel} v_b = \pm \omega_b \frac{k_{\parallel}}{k} J_0 \left(\frac{k_{\perp} v_{0\perp}}{\omega_c} \right). \quad (5)$$

Here ϵ is the linear dielectric constant, $k_{\parallel}' = k_{\parallel 1} - k_{\parallel 2}$, $v_{0\perp} = (2U_{\perp}/m_e)^{1/2}$, and $v_{tb} = (2T_b/m_e)^{1/2}$. The other notations are standard. It has been proved that E_{ω_1} , $E_{\omega_2} \rightarrow \infty$ at a finite time.² If $|[\alpha_1 |E_{\omega_1}(0)|^2 - \alpha_2 |E_{\omega_2}(0)|^2] t| \ll 1$, E_{ω_1} and E_{ω_2} can be expressed in simple forms which are useful for comparison with experimental measurements:

$$|E_{\omega_1}(t)/E_{\omega_1}(0)| = 1 + \beta_1 t, \quad (6)$$

$$|E_{\omega_2}(t)/E_{\omega_2}(0)| = 1 + \beta_2 t, \quad (7)$$

where the linear damping is neglected, $\beta_1 = \frac{1}{2}\alpha_2 \times |E_{\omega_2}(0)|^2$ and $\beta_2 = \frac{1}{2}\alpha_1 |E_{\omega_1}(0)|^2$.

In the experiments a monoenergetic beam with energy $U_b = 240$ – 270 eV and $I_b = 7$ – 8 mA (temperature $T_b \approx 0.5$ eV, transverse energy $U_{\perp} \approx 2$ eV,

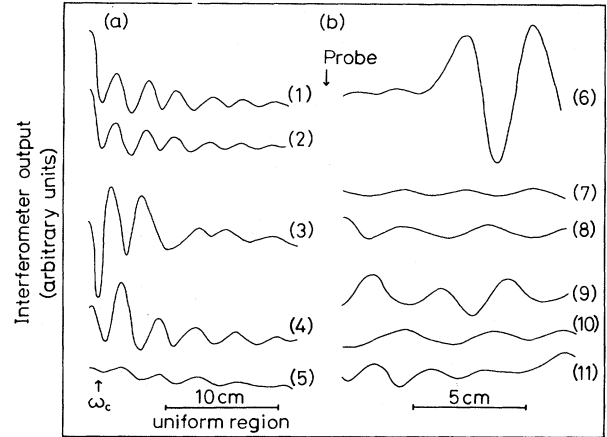


FIG. 1. (a) Interferometer traces in an inhomogeneous magnetic field. $\omega_1/2\pi = 405$ MHz; $\omega_2/2\pi = 320$ MHz; $\omega_c/2\pi = 153$ MHz; $U_b = 258$ eV; $I_b = 8$ mA; $V_1 = 0.03$ V [traces (1) and (2)], and $V_2 = 0.16$ V [traces (3)–(5)]. (b) Interferometer traces in a uniform magnetic field. $\omega_1/2\pi = 400$ MHz; $\omega_2/2\pi = 292$ MHz; $\omega_c/2\pi = 142$ MHz; $U_b = 265$ eV; $I_b = 7$ mA; $V_1 = 0.014$ V [traces (6)–(8)], and $V_2 = 0.022$ V [traces (9)–(11)].

diameter $D \approx 6$ mm) is continuously injected along a magnetic field into a beam-generated plasma (diameter ≈ 30 mm) at the argon gas pressure of 0.3 mTorr. The collision frequency of beam electrons is $\nu_e \approx 5 \times 10^6$ sec⁻¹, giving a mean free path of 2 m. The transverse energy of the beam is produced by the magnetic cusp in front of the electron gun or its slight inclination. On opposite side of the electron gun, a Faraday cup is placed to measure the parallel energy U_{\parallel} , and $U_{\perp} (=U_b - U_{\parallel})$ and T_b . Two coaxial antenna probes, axially and radially movable, are placed in the beam in order to detect and launch the waves.

In Fig. 1(a) we exhibit typical interferometer traces of two nonlinearly unstable waves. Two external signals with the frequencies ω_1 and ω_2 (voltages $V_1, V_2 \approx 0$ – 3 V) are applied to one of the electrodes of the gun, and the explosive instability occurs in the region near the gun where the magnetic field is inhomogeneous. Traces (1) and (2) show the first wave in the presence ($V_2 = 0.36$ V) and absence of the second external signal (ω_2), respectively. It is found that the first wave is slightly enhanced by the second external signal. Traces (3)–(5) show the second wave. Similarly, it is found that traces (3) and (4) in the presence of the first external signal ($V_1 = 1.55, 0.4$ V) are strongly enhanced compared with trace (5) without the first external signal, and that the wavelength of the second wave is shortened by the

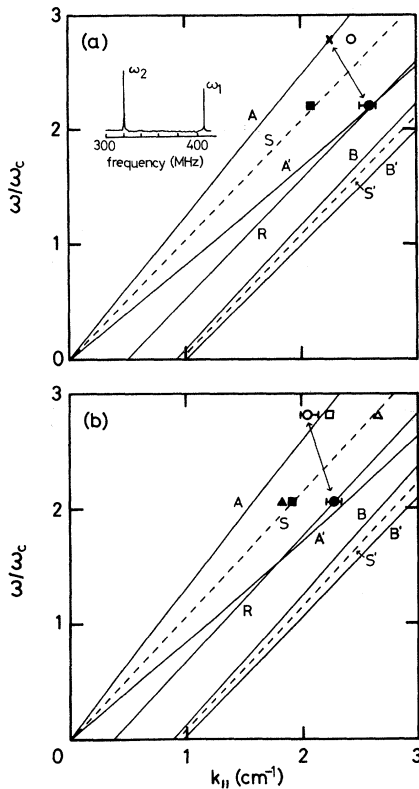


FIG. 2. (a) Location of traces in Fig. 1(a) on the dispersion diagram. The empty circle corresponds to traces (1) and (2), the full circle to traces (3) and (4), and the full square to trace (5). The solid lines A and A' show the fast and slow beam modes given by Eq. (5) under present experimental condition, respectively. The dotted lines S and S' indicate the space-charge and cyclotron waves of the beam in the limit $\omega \gg \omega_b$, respectively. (b) Location of traces in Fig. 1(b) on the dispersion diagram. The empty circle, square, and full triangle correspond to traces (6)–(8), respectively, and the full circle, square, and empty triangle to traces (9)–(11), respectively. The other explanations are similar to those in (a).

first external signal.

In Fig. 2(a), we show the location of traces in Fig. 1(a) on the dispersion diagram and the frequency spectrum showing the second wave enhanced by the first wave.⁸ We determine that the first wave is the fast beam mode, the second wave in the presence of the first wave is the slow beam mode, and the second wave in the absence of the first wave is a result of interference between the fast and slow beam modes.⁶ The straight line R exhibits the resonant condition Eq. (1), where $(\omega_1, k_{||1})$ are given by the theoretical dispersion relation A (shown by the cross), $m=1$, and the values of ω_c at the point shown by the ar-

row in Fig. 1(a) is used. We have confirmed that the second wave was not the linearly unstable wave (positive-energy one) due to a linear beam-plasma interaction. For comparison, the dispersion relation of the cyclotron waves of the beam given⁷ by $\omega - k_{||}v_b + \omega_c = \pm \omega_b(k_{||}/k)J_1(k_{\perp}v_{0\perp}/\omega_c)$ is shown by the solid lines B and B' ($k_{\perp} \approx 4.8/D$). It can be seen that the second wave is distinguished from the cyclotron wave of the beam B which is the positive-energy wave. We can conclude that the fast and slow beam modes are simultaneously amplified by the nonlinear interaction with the helical electron beam. These instabilities are caused more easily in an inhomogeneous region of the magnetic field than in a uniform region. However, there is uncertainty in the confirmation of the resonant condition due to the uncertainty in the value of ω_c .

We have tried to cause this instability in the uniform region of the magnetic field (1% in uniformity and 10 cm in length). In Fig. 1(b), we exhibit the typical interferometer traces obtained in the uniform region. By applying the second external signal to the gun and the first one to the probe located in the uniform region, we obtained traces (6)–(8) which show the first wave with $V_2=1.5$ V, the first one without the second one, and the second one, respectively. The first wave is enhanced and its wavelength stretches by the presence of the second wave, which means that only the fast beam mode grows. On the other hand, traces (9)–(11) were obtained by applying the first external signal to the gun and the second one to the probe, and show the second wave with $V_1=10$ V, the second one without the first one, and the first one, respectively. The second wave is also enhanced and its wavelength is shortened by the presence of the first wave, which means that only the slow beam mode grows. In Fig. 2(b), we show the location of traces in Fig. 1(b) on the dispersion diagram. We can also confirm the similar amplification of two beam modes in the uniform magnetic field. Moreover, we could observe the virtual wave at the difference frequency $\omega_1 - \omega_2$.

In Fig. 3(a) [3(b)], we show semilogarithmic plots of the first- (second-) wave power and a linear plot of the second- (first-) wave power versus the power of the second (first) external signal P_2 (P_1). We see that the first or second wave grows exponentially before saturation with increasing P_2 , or P_1 , respectively, and this amplitude variation follows the theoretical prediction^{4,6} ($e\varphi/T_b \lesssim 10^{-2}$).

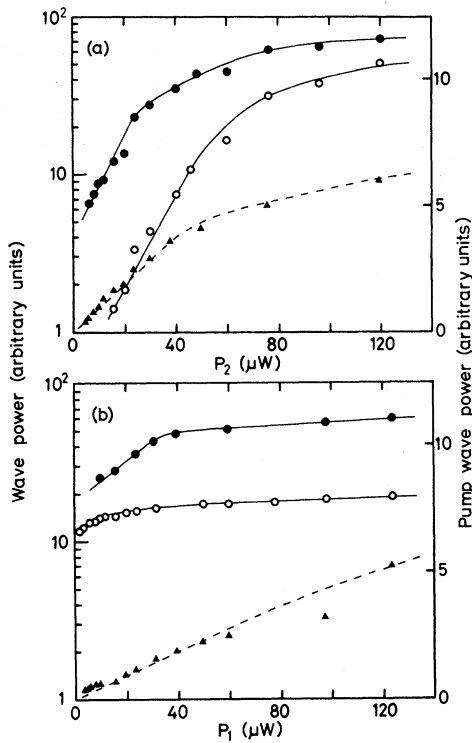


FIG. 3. (a) First-wave power vs P_2 is shown by the full and empty circles for the cases of $V_1=0.8$ and 0 V, respectively. The dotted line is a linear plot of the second- (pump-) wave power. (b) Second-wave power vs P_1 is shown by the full ($V_2=0.9$ V) and empty ($V_2=0$ V) circles. The dotted line is the first- (pump-) wave power. $\omega_1/2\pi=400$ MHz; $\omega_2/2\pi=292$ MHz; $\omega_c/2\pi=144$ MHz; $U_b=240$ eV; and $I_b=7$ mA.

In order to determine the nonlinear wave-particle coupling coefficients, the growth rate of the amplified waves β_1 and β_2 were measured. By the pulsative injection of the first external signal, as shown by the lower trace in the insets of Fig. 4(a) and the continuous injection of the second external signal to the gun, the time evolution of the first wave observed in the inhomogeneous region of the magnetic field was obtained with use of the boxcar detector, and its typical raw data are shown in the insets. From the upper trace, we see that the first wave grows initially and then saturates. We can regard the initial growing to be almost linear, as predicted by Eqs. (6) and (7). Similarly, the time evolution of the second wave was observed, and its typical raw data are shown in the insets of Fig. 4(b). The growth rate β_1 (β_2) obtained from the initial time evolution is plotted versus P_2 (P_1) in Fig. 4(a) [4(b)]. We can confirm that both β_1 , β_2 are proportional to P_2 , P_1 within the experimental error, respectively, and

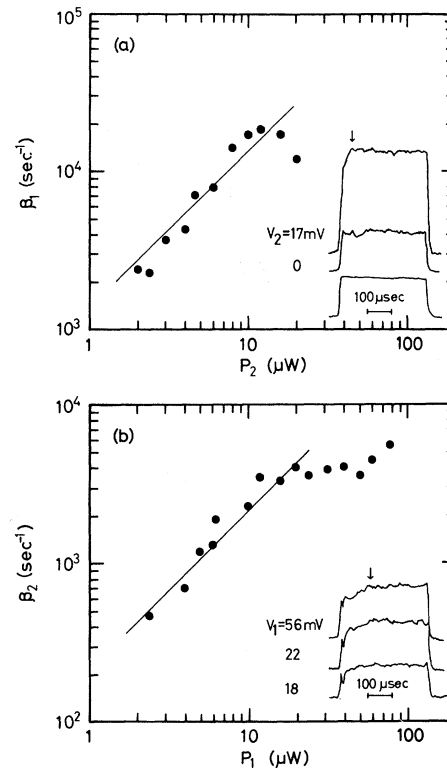


FIG. 4. (a) Growth rate of the first-wave β_1 vs P_2 with $V_1=3$ V. The arrow in the insets indicates the saturating point. (b) Growth rate of the second-wave β_2 vs P_1 with $V_2=0.7$ V. $\omega_2/2\pi=400$ MHz; $\omega_1/2\pi=292$ MHz; $\omega_c/2\pi=143$ MHz; $U_b=256$ eV; and $I_b=8$ mA.

this agrees qualitatively with the theoretical prediction.⁹ We estimated the electric field by measuring probe coupling coefficient, which is determined by the method described by Malmberg and Wharton.¹⁰ Thus, we obtained the coupling coefficients $\alpha_1 \approx 3.2 \times 10^{12}$ cm sec g^{-1} , $\alpha_2 \approx 7.2 \times 10^{12}$ cm sec g^{-1} from Fig. 4. The corresponding theoretical values obtained from Eq. (4) under the present experimental condition¹¹ are $\alpha_1 \approx 3.0 \times 10^{12}$ cm sec g^{-1} , $\alpha_2 \approx 3.4 \times 10^{12}$ cm sec g^{-1} . We consider this agreement to be good within the experimental error.

In conclusion, we believe that we have observed the explosive instability due to nonlinear wave-particle interaction.

(a) This work was partially supported by a Grant-in-Aid from the Ministry of Education in Japan.

¹C. T. Dum and E. Ott, Plasma Phys. **13**, 177 (1970).

²M. Porkolab and R. P. H. Chang, Phys. Fluids **15**, 283 (1972).

- ³S. Nakamura, J. Phys. Soc. Jpn. **42**, 280 (1977).
⁴R. P. H. Chang and M. Porkolab, Phys. Rev. Lett. **25**, 1262 (1970).
⁵K. W. Gentle and A. Malein, Phys. Rev. Lett. **26**, 625 (1971); H. Ikezi and Y. Kiwamoto, Phys. Rev. Lett. **27**, 718 (1971).
⁶R. Sugaya, M. Sugawa, and H. Nomoto, Phys. Fluids **19**, 1829 (1976), and J. Phys. Soc. Jpn. **42**, 1373 (1977).
⁷M. Seidl, Phys. Fluids **13**, 966 (1970).
⁸The frequency spectrum of Fig. 2(a) is the most simple form of a more detailed frequency spectra of the experiment.
⁹This means that it is not necessary to take into ac-

count the linear damping rate γ , although the collisional damping rate ν_e is greatly larger than β_1 and β_2 .

¹⁰J. H. Malmberg and C. B. Wharton, Phys. Rev. Lett. **19**, 775 (1967).

¹¹The theory in this Letter is only applicable to an infinite uniform plasma in a uniform magnetic field, but in the theory of finite and nonuniform plasma it is sufficient to alter only α_1 and α_2 . The accurate theoretical values of α_1 and α_2 cannot be obtained, because the accuracy of the values of plasma parameters is poor. Therefore, we compared the experimental values of α_1 and α_2 with the theory which does not match completely to the practical experimental situation.

Ion Heating in ATC Tokamak in the Ion-Cyclotron Range of Frequencies

H. Takahashi, C. C. Daughney, R. A. Ellis, Jr., R. J. Goldton, H. Hsuan, T. Nagashima,^(a) F. J. Paoloni, A. J. Sivo, and S. Suckewer
Plasma Physics Laboratory, Princeton University, Princeton, New Jersey 08540
 (Received 8 March 1977)

Ion heating by irradiation of rf fields in the ion-cyclotron range of frequencies is investigated using several diagnostic techniques. It is shown that substantial heating of the bulk of the ions can be achieved by this method.

It is generally believed that some form of supplementary heating will be required to heat tokamak plasmas to thermonuclear temperatures. One such method currently under intensive experimental¹⁻⁵ and theoretical⁶⁻¹¹ investigation is irradiation of the plasma by electromagnetic fields in the ion-cyclotron range of frequencies (ICRF heating). Although earlier heating experiments^{1,3,5} have produced encouraging results, it is not certain that the rf power can be deposited in the plasma in a meaningful manner by this method. In this Letter, results are reported from a recent series of experiments conducted in the adiabatic toroidal compressor¹² (ATC) near the second harmonic of the deuteron cyclotron frequency. These experiments extend the results of earlier efforts in the ST device⁵ by thorough investigation of the nature of the observed ion heating.

All heating experiments reported here are conducted with the second-harmonic resonance layer positioned near the center of the plasma. Moving the resonance layer in and out of the plasma shows that the wave-damping processes take place on or near the layer. However, the damping strength inferred from measured cavity Q factor is much stronger than expected from the second-harmonic resonant-damping theory. Similar observations were made in other experiments.³ The current theoretical model,⁸⁻¹¹ sup-

ported by some experiments,¹⁻⁴ is that the observed discrepancy is due to the influence of two-ion hybrid resonance between the majority deuterons and the minority protons. (The latter may be present in small quantities as impurities in a deuterium plasma.) However, the detailed mechanisms remain unclear, and this paper is primarily concerned with the investigation of power deposition.

The rf generator frequency (fixed at 25 MHz corresponding to the second-harmonic deuteron cyclotron frequency at 1.64 T) is matched well to the ATC device and the experiments can be conducted under favorable discharge conditions. Principally for this reason, the maximum rf energy input [limited by occurrence of magnetohydrodynamic (MHD) oscillations that often lead to plasma disruption] is one order of magnitude greater than for the ST experiments.⁵ The rf power and plasma parameters are adjusted to avoid these MHD oscillations. The rf power level (maximum peak power approximately 200 kW) drops during the pulse and all values quoted below refer to the time average. The pulse length (10 ms) is comparable or longer than the ion-energy replacement time (5-11 ms). It is considerably longer than various ion relaxation times (equipartition, deflection time, etc.) and the heating at the pulse end can be reliably assessed. This Letter presents strong evidence, substanti-